A mathematical model simulating the motion of the calcaneus from pressure plate measurements

EINDHOVEN UNIVERSITY OF TECHNOLOGY
Department of Mathematics and Computing Science

RANA 02-07
January 2002

A mathematical model simulating the motion of the calcaneus from pressure plate measurements

by

F. Hagman, S.J.L. v. Eijndhoven and A.A.F. v.d. Ven

Reports on Applied and Numerical Analysis
Department of Mathematics and Computing Science
Eindhoven University of Technology
P.O. Box 513
5600 MB Eindhoven, The Netherlands
ISSN: 0926-4507

A Mathematical Model simulating the Motion of the Calcaneus from Pressure Plate Measurements

Friso Hagman[a,b,*], Stef van Eijndhoven[a], Fons van de Ven[a]
[a] *Department of Mathematics and Computer Science, Technische Universiteit Eindhoven, The Netherlands*
[b] *Department of physical therapy and physical education, Vrije Universiteit Brussel, Brussels, Belgium*

Keywords: Foot kinematics, kinematical modelling, pressure plate systems, cinematography

Word Count: 2942

*Corresponding author. Address: Friso Hagman, Biomechanics Laboratory, Pleinlaan 2, 1050-Brussel (Belgium). Telephone number: +32/2.629.27.34. Fax number: +32/2.629.27.36 Email address: friso.hagman@vub.ac.be.

Abstract

This study simulates rearfoot motion during heel contact phase on the basis of pressure plate measurements. Kinematically, this motion is described as the rolling of a rigid object over a rigid plate. The model, describing this motion, was validated by comparing the simulated kinematics with cinematographically obtained three-dimensional kinematics. The results present a high degree of similarity between the Cardan angles obtained from both methods. Therefore, one may conclude that the pressure plate system can be used to reliably simulate rearfoot kinematics during heel contact.

Introduction

In the seventies and eighties of the last century, extensive studies on the lower extremity have been carried out based on measurements of two-dimensional nature obtained from high-speed cinematography (McClay et al., 2000). From these studies, it has been concluded that excessive subtalar pronation is linked to running-related injuries, and that the eversion of the calcaneus is a reliable predictor of the amount of pronation (Clarke et al., 1984, Van Gheluwe et al., 1999). Nowadays, the analysis of the rearfoot is performed using a three-dimensional approach. However, improving the approach from two-dimensional to three-dimensional did not alter the conclusion that excessive subtalar pronation is linked to running-related injuries (Lundberg et al., 1989). In this study, instead of analysing the motion of the rearfoot by means of cinematography, a pressure plate system is used. In the case of cinematography, there is a direct link between the temporal measurements and the motion of the calcaneus. In the case of a pressure measurement system, there is no such link since not the motion itself is measured but the temporal pressure distribution resulting from the motion. So, additionally, a mathematical model is needed that links these pressure distribution measurements to calcaneal motion. Furthermore, the motion of the calcaneus can be described only when heel and plate are in contact with each other. This is a limitation of the use of a pressure measurement system. The mathematical model mentioned above, uses the pressure distribution as input to the model. The pressure distribution, at each measurement time point, is used to compute the temporal path of the centre of pressure (CoP). This temporal path is the basis of our mechanical model, since the motion is mechanically described as the rolling of the rigid calcaneus over a rigid plate, where the CoP at each instance is the contact point. Thus, while the input to the model is the temporal pressure distribution, the output of the model is the motion of the calcaneus in the three cardinal planes with respect to a fixed reference frame.
Because of the used input, a mathematical tool has been developed that relates input to desired output. The approach taken to link plantar pressure distribution to rearfoot kinematics differs from all other approaches so far. Models found in literature either calculate foot kinematics on the basis of cinematography (Areblad et al.; 1990, Scott et al.; 1993, McClay et al.; 1998), or describe foot kinematics (and kinetics) on a purely theoretical basis (Salathé et al.,; 1986, Morlock et al.; 1990, E. Forster et al.; 2000). There seems to be no literature available that uses pressure plate measurements as direct input to a kinematical model.
Therefore, the purpose of this study is to simulate three-dimensional rearfoot kinematics during heel contact solely from pressure plate measurements.

Model

Description of the Model
The mathematical model is built upon the following three points: it uses the measurements from a pressure measurement system as input, it contains the mathematical equations describing contact between heel and plate, and it produces the temporal orientation of the calcaneus in terms of Cardan angles, see Figure 1.

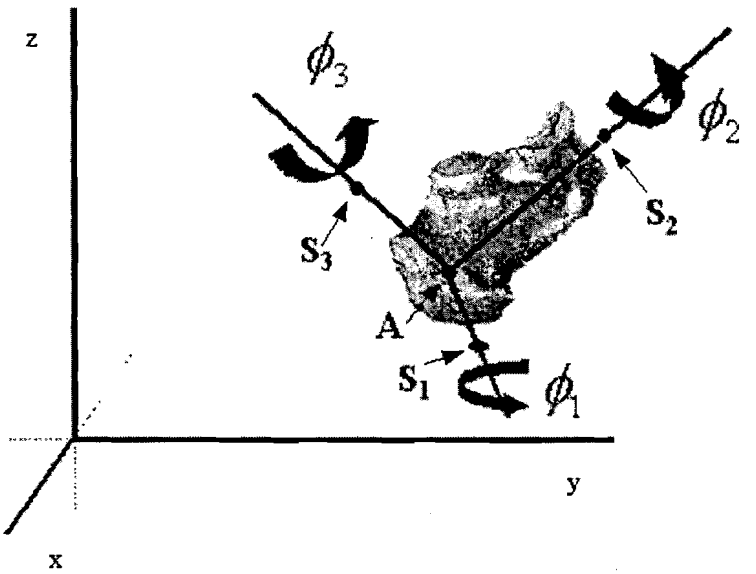

Figure 1: The calcaneus reference frame with respect to the plate reference frame {Oxyz}. The angles φ_1, φ_2 and φ_3 are the Cardan angles, and the points A, S_1, S_2, and S_3 span the calcaneus reference frame.

In the first step, the heel in contact with the plate is considered a four-layer system: the calcaneus, the soft tissues between calcaneus and plate, the elastic layer of the plate, and the rigid layer of the plate, see Figure 2. Top and bottom layer are rigid layers, while intermediate layers are elastic. The elastic layer transfers the forces exhibited by the calcaneus on the pressure plate into a temporal pressure distribution over a finite contact area. This pressure distribution, at each measurement time point, is used to compute the temporal path of the centre of pressure (CoP).

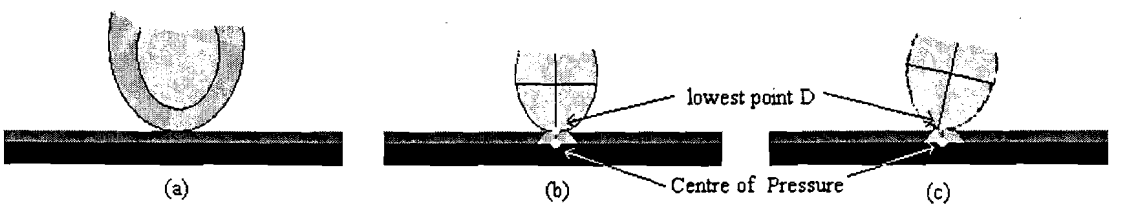

Figure 2: (a) the four-layer system, where the calcaneus is depicted in light grey and the rigid layer of the plate is depicted in black. In (b) and (c), a graphical interpretation of step two is given, where (b) en (c) are taken as different subsequent time steps. The distance between point D and the Centre of Pressure is equal in both (b) and (c). The light grey area within the elastic layer shows the influence of this layer on the measured pressure distribution.

In the second step, the two intermediate layers are considered as one layer on top of the plate. This makes sense because the elastic properties of the plate layer do not influence the pressure distribution measurement to the same extent as the soft tissue layer does.

In the third step, the further influences of the elastic layer are neglected, thus obtaining a rigid contact system. Assuming local concavity of the calcaneal surface, there exists a point on the plate having minimum distance to the calcaneal surface, see Figure 2. This point is taken to coincide with the computed CoP. Moreover, changes in this minimum distance are assumed to be small in comparison to the global motion of the calcaneus. Therefore, this distance is taken constant during heel contact. All this results in a rolling problem for a rigid body, see Figure 3.

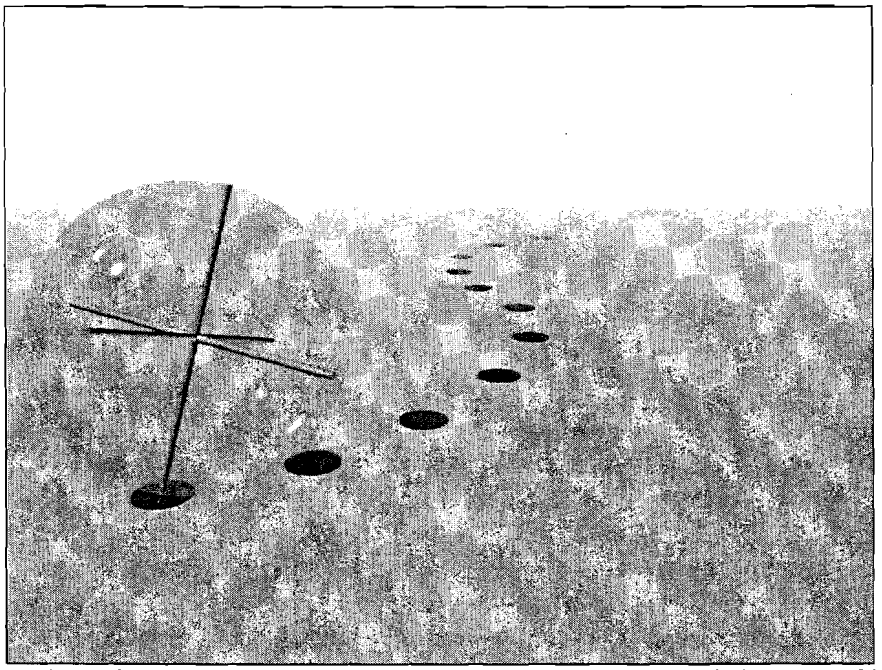

Figure 3: A rigid sphere with a comoving coordinate system rolling over a rigid plate (created by J. Gaublomme).

Assumptions

In the previous part, the steps towards getting from the 'real world system' to the artificial rigid system were explained. In this process, assumptions were made, not all of them explicitly mentioned, such as.

- The calcaneus is assumed to be rigid.
- Elasticity of the soft tissues surrounding the calcaneus results in a finite area of pressure distribution.
- The calcaneal surface is locally concave.
- At each time point, the calcaneus has a point of minimal distance to the plate. The latter two items come down to the assumption that the distance between calcaneus and plate can be regarded constant during heel contact in comparison to the magnitude of the motion of the calcaneus.
- The temporal CoP path coincides with the path described by the projection onto the plate of the lowest point of the calcaneus during motion.
- The calcaneus does perform no spin with respect to the axis normal to the plate. Spin motion cannot be measured by a pressure plate system.

Input – Model – Output

Essential in the model is the simulation of calcaneal motion through solving the problem of a rolling rigid body.
The motion of the calcaneus is determinated by the aforementioned Cardan angles. To be able to calculate these angles, there is need for a fixed laboratory reference frame and a comoving, or local, reference frame. The fixed laboratory reference frame is attached to the plate; where x- and y-axis are chosen parallel to the horizontal plane of the plate, and the z-axis is perpendicular to the plate, see Figure 1. The motion of the local reference frame is determined by the kinematical equation (2), which is a first order differential equation in time, t. So, this motion is known, if the local reference frame at a certain time point is (the initial conditions). The Cardan angles ($\varphi_1(t_k)$, $\varphi_2(t_k)$, and $\varphi_3(t_k)$) at measurement time point t_k follow from the transformation matrix $\mathbf{T}(t_k)$ that describes the transformation from the local reference frame to the fixed laboratory reference frame at each time point t_k (Wittenburg, 1977, pp 19-25).

$$\mathbf{T}(t_k) = \begin{bmatrix} c_2c_3 & c_1s_3 + s_1s_2c_3 & s_1s_3 - c_1s_2c_3 \\ -c_2s_3 & c_1c_3 - s_1s_2s_3 & s_1c_3 + c_1s_2s_3 \\ s_2 & -s_1c_2 & c_1c_2 \end{bmatrix}, \tag{1}$$

where $c_i = \cos(\varphi_i(t_k))$, $s_i = \sin(\varphi_i(t_k))$, $i = 1,2,3$, and $k = 1,...,N$.
So, if the transformation matrix $\mathbf{T}(t_k)$ is known, the Cardan angles associated with the transformation can be calculated with the use of relation (1). The calculation of this transformation matrix concludes the following part, and embodies the link between the problem of rolling rigid bodies and the stated objective.

Model Equations
To describe the motion of the local reference frame attached to the calcaneus with respect to the fixed laboratory reference frame, the positions of four points spanning this frame must be known (see Figure 1, points A, S_1, S_2 and S_3) at every measurement time point. The fundamental law of kinematics (see equation (2)) can be used to calculate the positions of these four points. The fundamental law states that the velocity of each point P of a rigid body, described by the position vector $\vec{x}_P$, satisfies

$$\vec{v}_P = \vec{v}_A + \vec{\omega} \times \vec{y}_P, \tag{2}$$

where $\vec{v}_A$ denotes the velocity of the point A of the rigid body, $\vec{\omega}$ denotes the angular velocity, and $\vec{y}_P = \vec{x}_P - \vec{x}_A$, where $\vec{x}_A$ denotes the position vector of point A.

A discretisation of the first order differential equation $\vec{v}_P = \frac{d}{dt}\vec{x}_P$ yields

$$\vec{x}_P(t_{k-1}) = \vec{x}_P(t_k) - \Delta t\, \vec{v}_P(t_k), \tag{3}$$

where Δt is the time step, and $t_k = k\Delta t$.
The fundamental law yields

$$\vec{v}_P(t_k) = \vec{v}_A(t_k) + \left(\vec{\omega}(t_k) \times [\vec{x}_P(t_k) - \vec{x}_A(t_k)]\right). \tag{4}$$

In our case, the positions of the points S_1, S_2, and S_3 are calculated using the recurrence relation (3) combined with equation (4). However, before equation (3) can be used, the following unknowns have to determine

$$\vec{v}_A(t_k), \vec{\omega}(t_k), \text{ and } \vec{x}_A(t_k).$$

For this, the fact that the contact point has zero velocity is used. Thus, it is obtained that

$$\vec{v}_A(t_k) = -\vec{\omega}(t_k) \times \vec{y}_{CoP}(t_k), \tag{5}$$

where $\vec{y}_{CoP}(t_k) = \vec{x}_{CoP}(t_k) - \vec{x}_A(t_k)$, and $\vec{x}_{CoP}(t_k)$ is the position vector of the CoP, which is momentarily coinciding with the contact point. In this way, a relation between $\vec{v}_A(t_k)$ and $\vec{\omega}(t_k)$ is established, reducing the number of unknowns to two: $\vec{x}_A(t_k)$ and $\vec{\omega}(t_k)$.

For $\vec{x}_A(t_{k-1})$, the approximation (3) for point A is used:

$$\vec{x}_A(t_{k-1}) \cong \vec{x}_A(t_k) - \Delta t \vec{v}_A(t_k). \tag{6}$$

What remains is the calculation of the angular velocity at time t_k, $\vec{\omega}(t_k)$. This calculation is performed with the use of differential geometry and results in the following theorem:

Theorem 1 *Let a rigid body B be rolling over a rigid plate such that the points of contact between the rigid body and the plate form a smooth path, $\vec{x}(t)$, $t \in [T_b, T_e]$. Let at time point t_P, the material point P of B be the point of contact between the rigid plate and rigid body, with position $\vec{x}(t_p)$. Then the angular velocity of the rigid body at time point t_P, $\vec{\omega}(t_P)$, is given by*

$$\vec{\omega}(t_P) = \vec{\vec{S}}|_P \left(\frac{d}{dt} \vec{x}(t_p) \times \vec{n}|_P \right), \tag{7}$$

where $\vec{\vec{S}}|_P$ is the curvature tensor at point P, and $\vec{n}|_P$ is the outward normal at point P, on the surface of B.
A proof of this theorem can be found in Hagman, 2001.

So, with the use of equations (4), (5), (6), and (7), the right-hand side of the recurrence relation (3) is known completely. Therefore, after having determined the position vectors $\overrightarrow{AS}_1(t_k), \overrightarrow{AS}_2(t_k)$ and $\overrightarrow{AS}_3(t_k)$ from recurrence relation (3), the orientation of the calcaneus reference frame is known in every measurement time point. In turn, these vectors are used to calculate the transformation matrix, from its definition

$$\mathbf{T}(t_k) = \left[\frac{\overrightarrow{AS}_1(t_k)}{\left\| \overrightarrow{AS}_1(t_k) \right\|} ; \frac{\overrightarrow{AS}_2(t_k)}{\left\| \overrightarrow{AS}_2(t_k) \right\|} ; \frac{\overrightarrow{AS}_3(t_k)}{\left\| \overrightarrow{AS}_3(t_k) \right\|} \right], \tag{8}$$

and from this the Cardan angles, using the relations $\varphi_i(t_k) = \arcsin(s_i)$, $i = 1,2,3$.

Still one problems remains: the geometry of the calcaneus by which $\vec{\vec{S}}|_P$ and $\vec{n}|_P$ should be determined. Assuming that at time t_k and in the neighbourhood of the contact point, this geometry is a sphere with radius $R(t_k)$, one can determine the Cardan angles in a straightforward manner, using

$$\vec{x}_{CoP}(t_k) = [C_x(t_k), C_y(t_k), 0] \tag{9}$$

$$\vec{x}_O(t_k) = [C_x(t_k), C_y(t_k), R(t_k)], \tag{10}$$

$$\vec{v}_O(t_k) = \frac{1}{\Delta t}[C_x(t_k) - C_x(t_{k-1}), C_y(t_k) - C_y(t_{k-1}), 0], \tag{11}$$

$$\vec{\omega}(t_k) = \frac{1}{R(t_k)\Delta t}[C_y(t_k) - C_y(t_{k-1}), -C_x(t_k) + C_x(t_{k-1}), 0]. \tag{12}$$

In the derivation of equation (12), it is used that for a sphere of radius R, $\vec{\vec{S}} = R\vec{\vec{I}}$, $\vec{\vec{I}}$ the unit tensor, and that $\hat{n}$ is the unit vector in the negative z-direction.
In the remainder of this paper, it is assumed indeed that locally the surface of the calcaneus coincides with the surface of a sphere. Scanning the calcaneal surface can validate this assumption.

Methods

To validate the output of the mathematical model, Cardan angles originating from the model should be compared with the golden standard, i.e. Cardan angles originating from cinematographical measurements. The sets of Cardan angles in this study were obtained from measurements, starting from heel impact and ending at forefoot contact. These temporal events were determined using the pressure plate: heel impact is defined to be the time point at which pressure is registered for the first time during a measurement trial, whereas the beginning of forefoot contact is defined to be the time point at which two percent of the total pressure is underneath the forefoot.
The measurements were performed with five subjects. For each subject, the left foot was measured in five trials, with the goal to obtain three trials for analysis.
In the remainder of this section, the properties of the measurement devices are highlighted: the calculations and analyses performed on the data, and the comparison of the two sets of Cardan angles obtained.

Devices
The conducted measurements combine the data from a camera set-up, a pressure plate system, and a force plate. More specifically:

- A camera set-up of six cameras positioned at the corner points of a hexagon. The MCU240 cameras were made by Qualisys, and measurements were performed at a frequency of 240Hz. A measurement volume of 70cm by 60cm by 55cm was chosen resulting in a residual camera calibration error of at most 0.7459 (average: 0.5542).
- A footscan pressure plate of 200cm by 40cm constructed by RSscan International. The measurements were performed with a frequency of 480Hz. The number of sensors is 16384, and each sensor controls a rectangular region of 5mm by 7mm. The size of the sensor points is 3.5mm by 3.5mm.
- A force plate of 200cm by 40cm constructed by Amti. The measurements were performed at a frequency of 1200Hz. The force plate was used to calibrate the pressure plate, dynamically.
- A 3D data box constructed by RSscan International. The box triggers all measurement devices at the same time, thus enabling synchronisation of the start time point of the measurements for all devices.

Camera measurements and data analysis
To be able to calculate the Cardan angles from cinematography, a specific marker setting was adapted from McClay et al., 1998. The McClay setting uses markers to define the segments, the so-called anatomical markers, and markers to track the motion, the so-called tracking markers. Two anatomical markers were attached to the lateral and medial side of the calcaneus, and two others were placed on the heads of the first and fifth metatarsal bone. As tracking markers were used the lateral and medial markers on the calcaneus, and one marker positioned on the insertion of the calcaneus. First, a static trial was performed with the complete marker setting, anatomical and tracking. Afterwards the dynamic trials were performed without the anatomical markers on the metatarsal heads.
Cardan angles were calculated with the software package Move3D from the National Institutes for Health. Input for this software package is a dynamic trial, a static trial, and a so-called model file that describes the foot segment. With these files, Move3D constructs a reference frame for the foot segment such that rotation about the anterior-posterior axis of the segment is used to describe calcaneal inversion/eversion, the medial-lateral axis is used to describe plantar flexion / dorsal flexion, and the inferior-superior axis is used to describe abduction/adduction. The output of Move3D is an ASCII file containing the three angles at a series of time points.

Pressure measurements and data analysis
In the case of a dynamic trial, the pressure distribution was measured and exported to an ASCII file, subsequently. In the mathematical programming and analysis environment, Matlab, three procedures were developed to calculate the desired Cardan angles on the basis of the mathematical models described: a procedure to load the exported ASCII file into the Matlab environment, a procedure to calculate the temporal path of the CoP, and a procedure to calculate the Cardan angles.

Validation method
Cardan angles obtained from cinematography combined with Move3D, and Cardan angles obtained from the pressure plate system combined with the mathematical model were compared in the Matlab environment.
Because the measurement frequencies of both systems were not the same, the cinematographical Cardan angles were interpolated with the use of a standard Matlab function for cubic splines.
Unfortunately, there is no method available yet to determine the radius of the sphere describing the calcaneus, locally. The problem was circumvented by equalising the *range* of the plantar flexion / dorsal flexion from both sources, in this way providing a value for the radius of the sphere.
Finally, the initial orientation of the calcaneus reference frame should be specified in the model equations. Naturally, the same initial orientation was chosen as the one following from the cinematographical data. This means that both sets of Cardan angles have the same end points (recall that the calculations are performed in backward order).

Results

With the use of the model equation, the Cardan angles can be calculated using input from the pressure plate system. As an example one is referred to Figure 4, where the

Cardan angles of two trials calculated with the model equations are depicted. All the other trials not mentioned as an example here are posted at the website of the Journal of Biomechanics. The two trials in Figure 4 are used throughout this section.

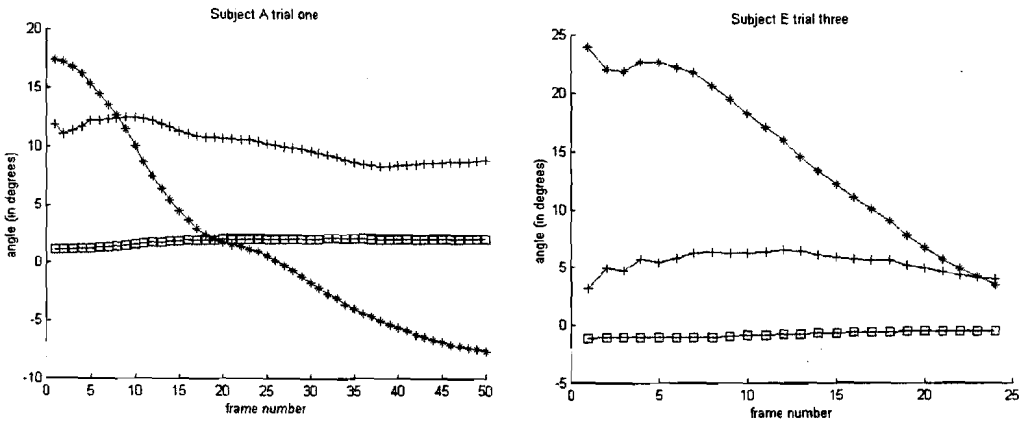

Figure 4: Cardan angles from two subjects obtained from pressure measurements combined with the mathematical model. In this figure, the stars denote the dorsal flexion / plantar flexion curve, the plusses denote the inversion /eversion curves, and the squares denote the abduction / adduction curves.

Figure 5 depicts the comparison between the sets of Cardan angles obtained from the cinematographical measurements and pressure measurements. As already said before, the Cardan angles of two different sets have the same initial condition resulting in equal end points of the curves.

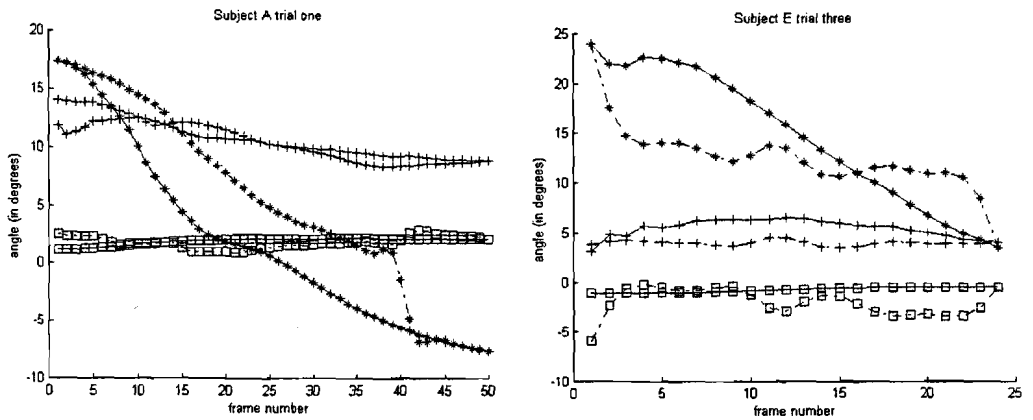

Figure 5: Comparison of Cardan angles obtained from the mathematical model and obtained from cinematography. In this figure, the stars denote the dorsal flexion / plantar flexion curve, the plusses denote the inversion /eversion curves, the squares denote the abduction / adduction curves. Moreover, the full line curves denote the model curves and the line-dot curves denote the cinematographical curves.

The Cardan angles from the model show a more realistic behaviour than the unsmoothed Cardan angles from the cinematographical measurements, because of the abrupt changes observed in the latter curves. Despite of this, the correspondence between the two results presents a high degree of similarity.

Next, the differences between the angles obtained from cinematographical measurements and the angles obtained from pressure measurements are calculated. These differences are depicted in Figure 6.

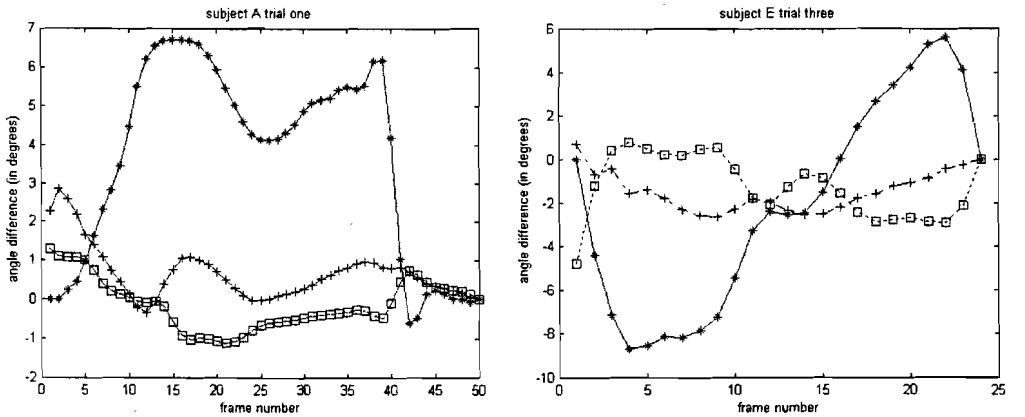

Figure 6: The differences in angles between the cinematographical and model results: stars denote the difference between the dorsal / plantar flexion curves, plusses denote the difference between the inversion / eversion curves, and squares denote the difference between the abduction / adduction curves.

Figure 6 shows plateaus alternated with a sudden rise or fall in the angular difference. This behaviour originates from so-called outliers in the cinematographical data, and influences the comparison due the selected criterion, namely equalising the ranges of the dorsal / plantar flexion curves. Therefore, it may be more appropriate to analyse the difference in trend between the sets of angles. This difference in trend is represented in Figure 7 by the differences in changes in the two sets of Cardan angles between two subsequent frame numbers

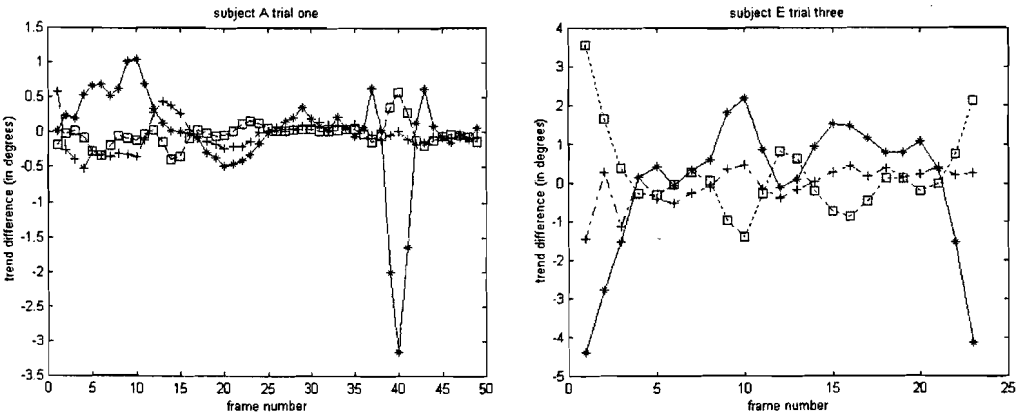

Figure 7: The trend between the cinematographic and model results: stars is the difference between the dorsal / plantar flexion curves, plusses is the difference between the inversion / eversion curves, and squares is the difference between the abduction / adduction curves.

Conclusions

The overall conclusion of this study is that a pressure measurement system enables us to reliably simulate the motion of the calcaneus, at least during the period from heel

impact up to forefoot contact. Thus, an alternative for determining the orientation of the calcaneus during heel contact is presented, yielding a reduction of measurement cost and (set-up) time.
Further, it is concluded that the assumptions, which are at the basis of the mathematical model are justified. Therefore, a first order approach, in which a sphere approximates the calcaneal surface, is valid. Furthermore, from the pressure measurement the temporal CoP path is needed only; no other aspects of the pressure distribution are taken into account. Finally, we observe that the CoP of a pressure distribution is less susceptible to measurement noise, than markers in a cinematographical measurement.

Acknowledgement

We would like to acknowledge prof. dr. D. de Clercq, head of the biomechanics laboratory of Universiteit Gent, for the use of the biomechanics laboratory and the constructive collaboration. Secondly, we acknowledge RSscan International, for providing us with the necessary measurement devices. Finally, we would like to acknowledge prof. dr. B. Van Gheluwe, head of the biomechanics laboratory of Vrije Universiteit Brussel, for his positive contribution with respect to this study.

References

[1] Salathe, E.P. jr., Arangio, G.A., Salathe, E.P., 1986. A biomechanical model of the foot. Journal of Biomechanics 19, 989-1001.

[2] Areblad, M., Nigg, B.M., Ekstrand, J., Olsen, K.O., Ekström, H., 1990. Three-dimensional measurment of rearfoot motion during running. Journal.f Biomechanics 23, 933-940).

[3] Clarke, T.E., Fredrick, E.C., Hamill, C., 1984. The study of rearfoot movement in running. In: E.C. Frederick (Ed.), Sport Shoes and Playing Surfaces, Human Kinetics Publishers, Champaign, 166-189.

[4] Hagman, F., 2001. Foot kinematics described from pressure plate measurements. Post graduate thesis, Mathematics for Industry, Eindhoven university press, Eindhoven.

[5] Morlock, M., Nigg, B.M., 1991. Theoretical considerations and practical results on the influence of the representation of the foot for the estimation of internal forces with models. Clinical Biomechanics 6, 3-13.

[6] Lundberg, A., 1989. Kinematics of the ankle and foot, Acta Orthop Scand Suppl 60:1.

[7] Scott, S.H., Winter, D.A., 1993. Biomechanical model of the human foot: kinematics and kinetics during the stance phase of walking. Journal.of Biomechanics 26, 1091-1104.

[8] McClay, I., 2001. The Evoulation of the Study of The Mechanics of Running; Relationship to injury. J. Am. Podiatr. Med Assoc 90(3), 133-148.

[9] McClay, I.,. Manal, K., 1998. Three-dimensional kinetic analysis of running: significance of secondary planes of motion. Medicine & Science in Sports & Exercise, 1629-1637.

[10] Forster, E., Muellner, T., Steffan, H., Geigl, B., 2000. Numerics simulation of the human ankle, the subtalar and the midtalar joints. In proceedings of the sixth International Symposium on the 3D Analysis of Human Movement. University of Cape town, South Africa.

[11] Van Gheluwe, B., Kewin, D., Roosen, Ph., Tielemans, R., 1999. The Influence of Heel Fit on Rearfoot Motion in Running Shoes. Journal of Applied Biomechanics 15, 361-372.

[11]Wittenburg, J., 1977. Dynamica of Systems of Rigid Bodies, Teubner, Stuttgart.

Appendix

In addition to the example figures provided in the article, the appendix consists of the same type of figures for every subject and every trial performed in this study.
In all figures, the main title refers to the subject and its trail. Furthermore, there are three graphs per figure: (A) the comparison between Cardan angles resulting from both the mathematical model and the cinematographical measurements, (B) The differences in angles between the cinematographical and model results, and (C) The trend between the cinematographic and model results.
With in this figures, the starts denote the plantar flexion / dorsal flexion curves, the plusses denote the inversion / eversion curves, the squares denote the abduction / adduction curves, and in (A) the full line curves denote the model curves and the line-dot curves denote the cinematographical curves.

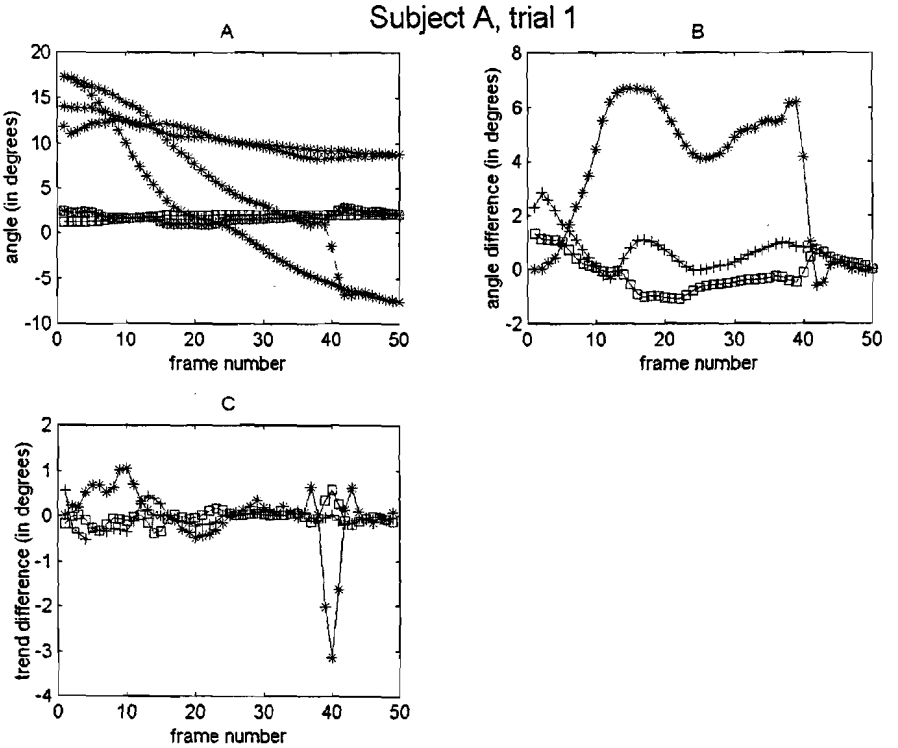

Subject A, trial 2

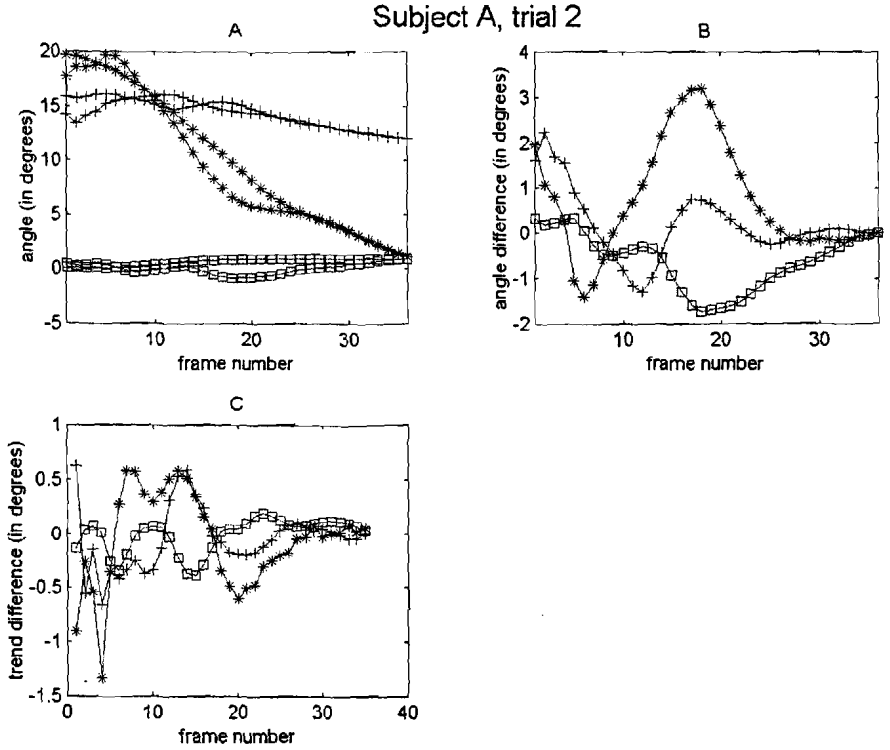

Subject A, trial 3

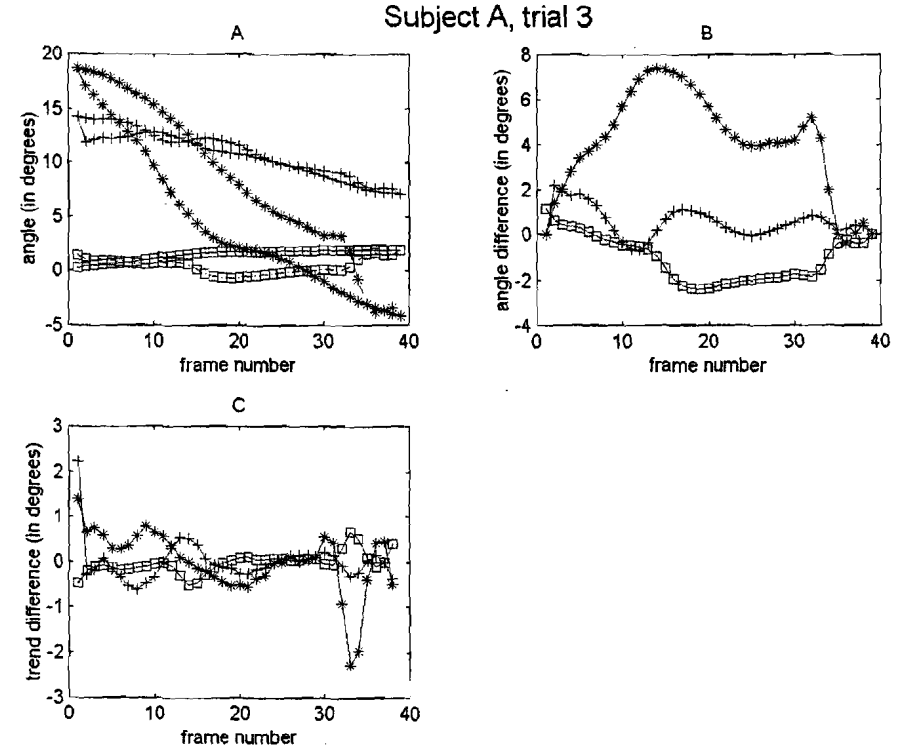

Subject A, trial 4

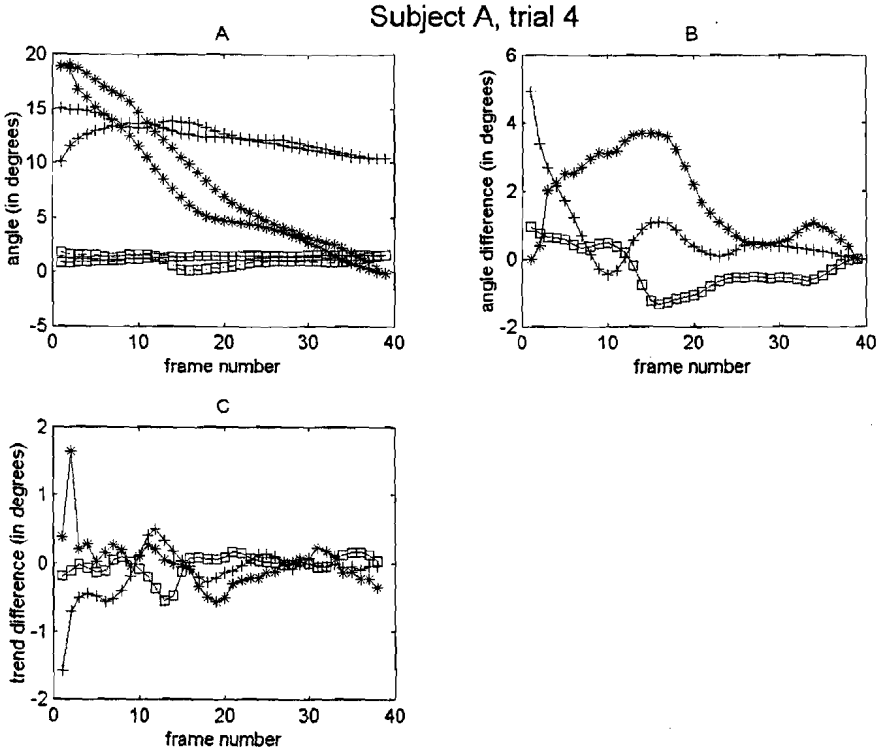

Subject A, trail 5

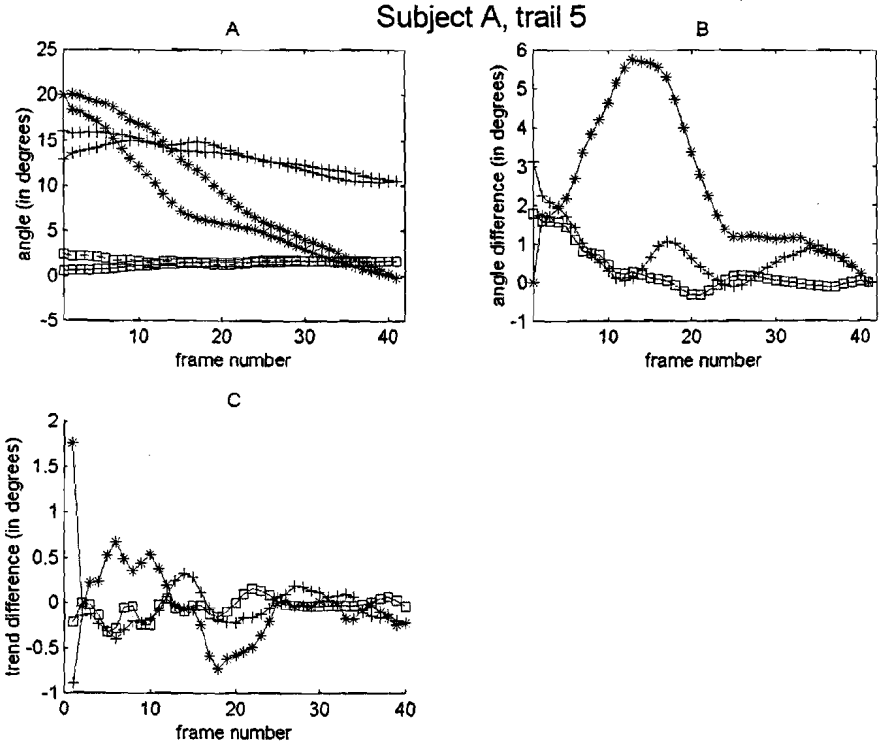

Subject B, trial 2

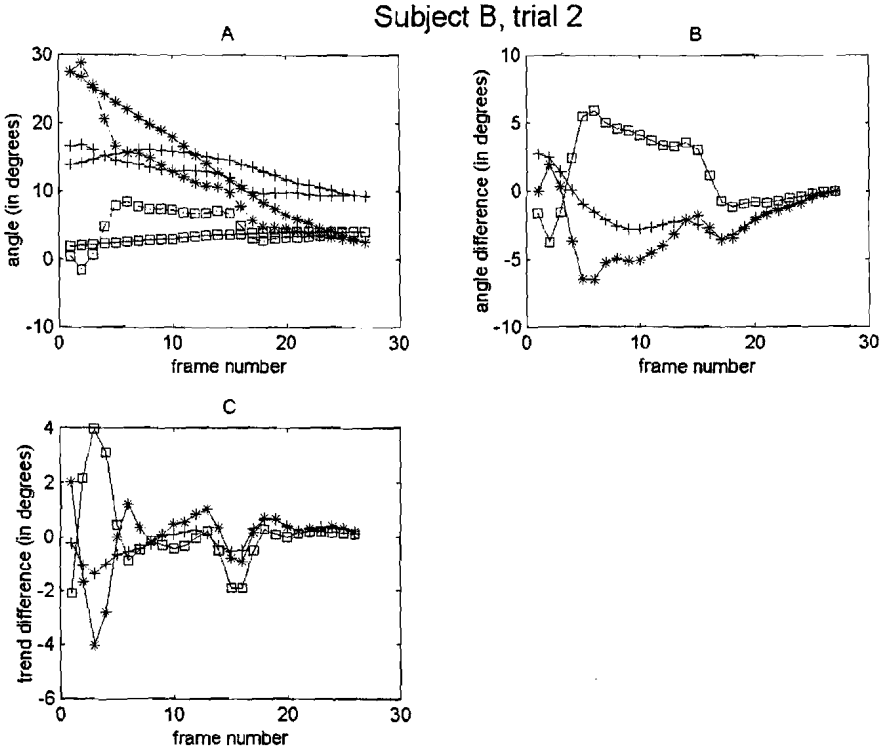

Subject B, trial 3

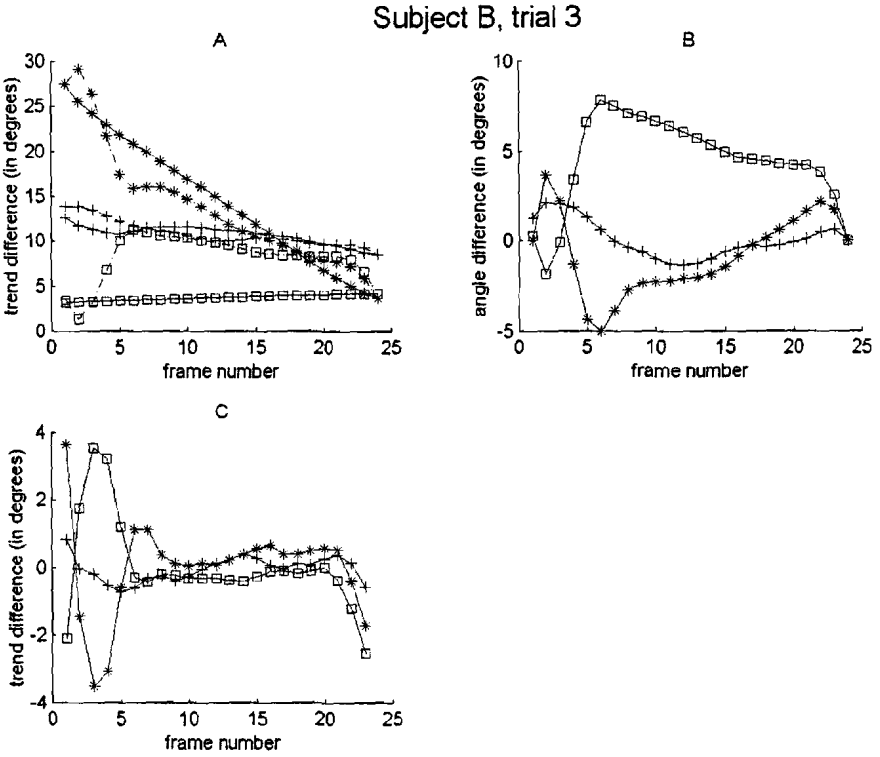

Subject B, trial 4

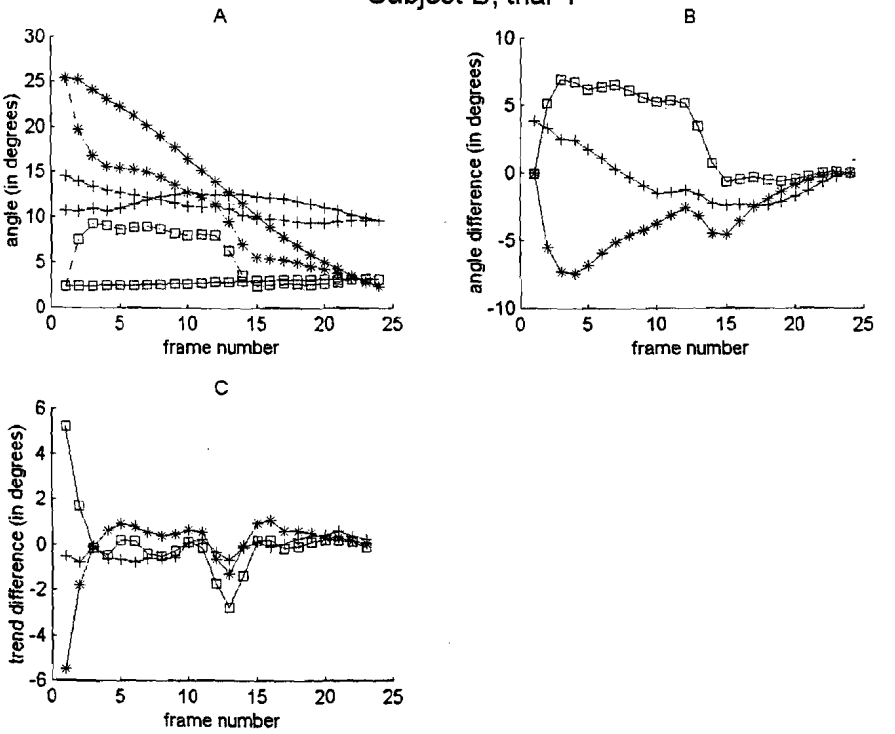

Subject B, trial 5

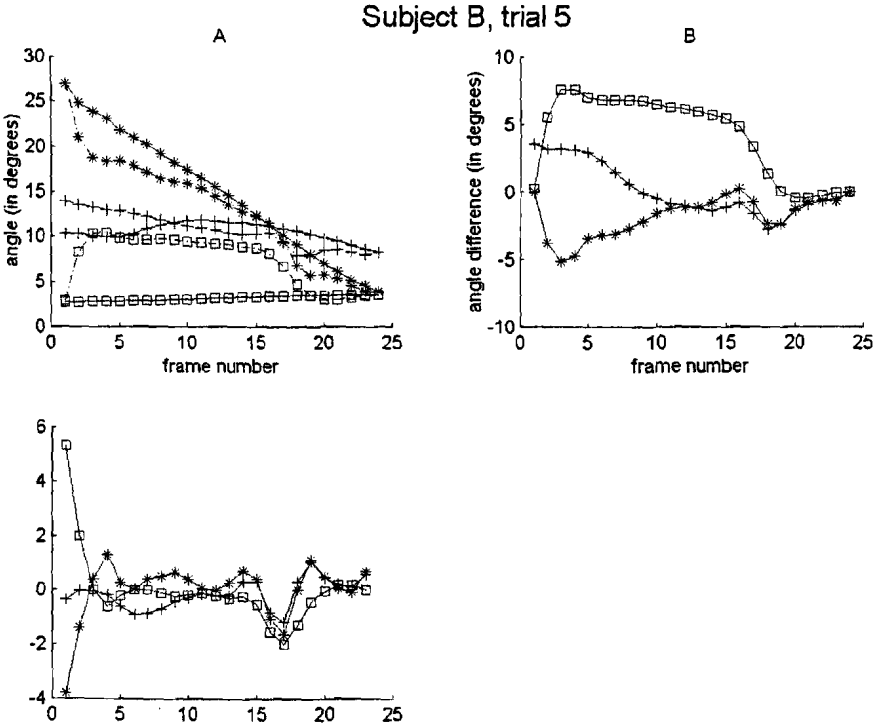

Subject C, trial 1

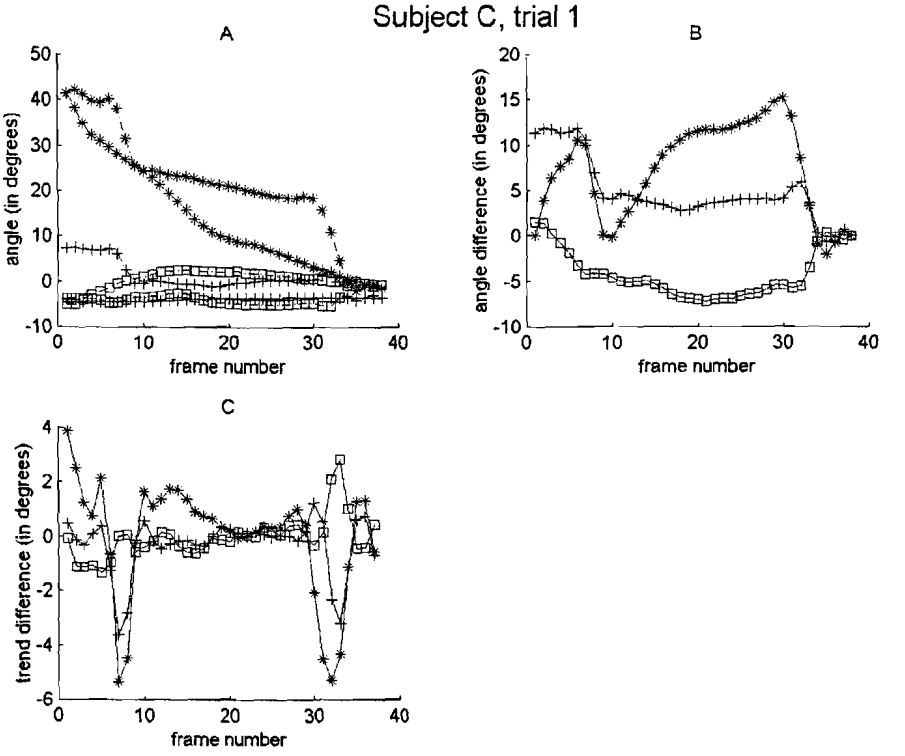

Subject C, trial 2

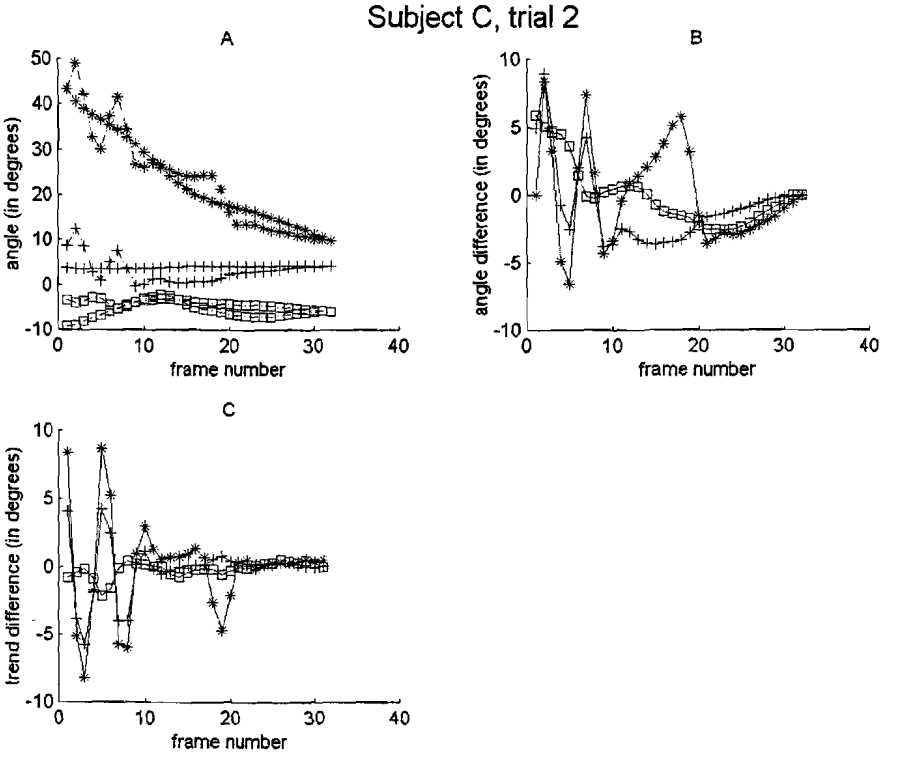

Subject C, trial 3

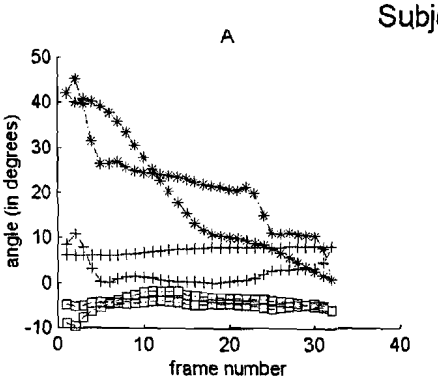

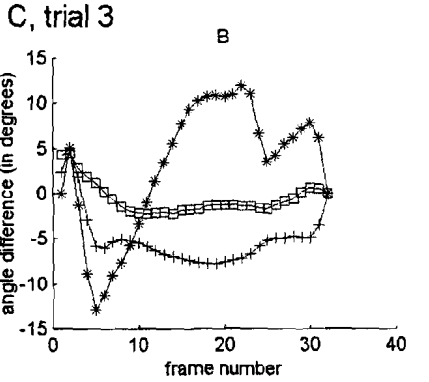

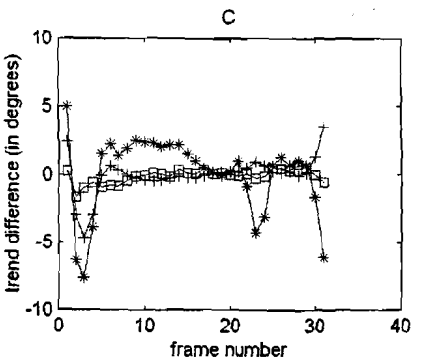

Subject C, trial 4

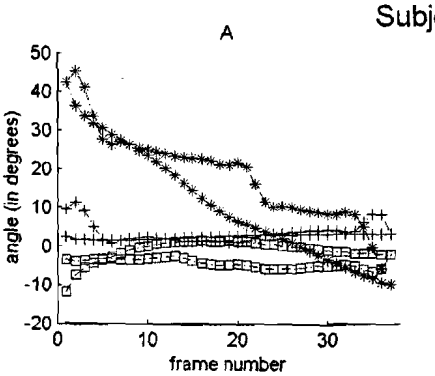

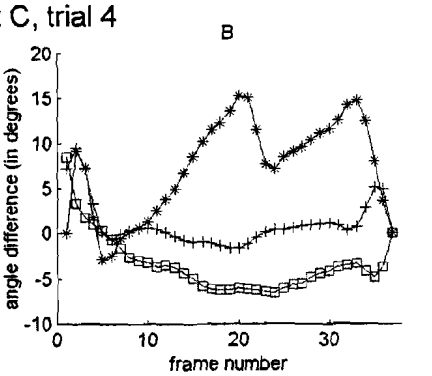

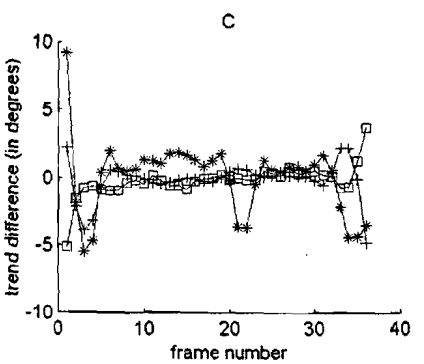

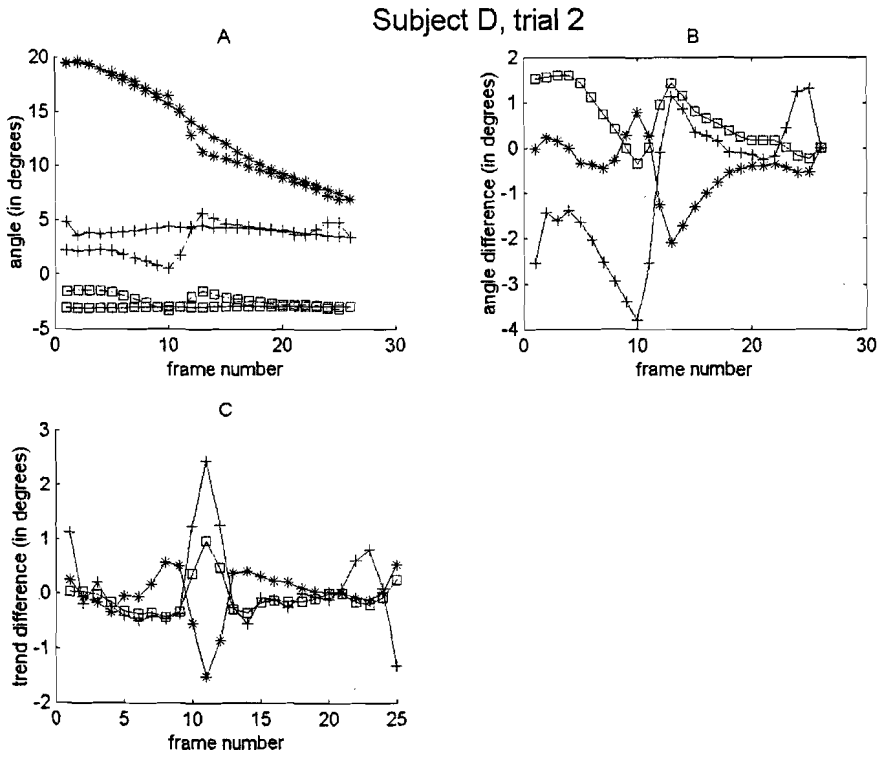
Subject D, trial 2
A
B
C
angle (in degrees)
angle difference (in degrees)
trend difference (in degrees)
frame number

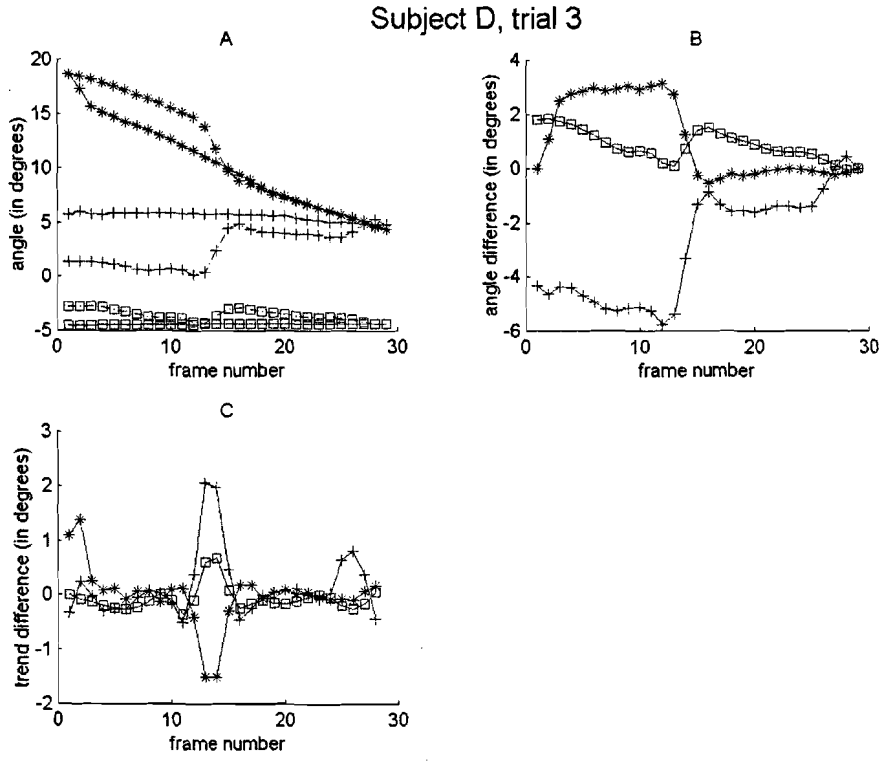
Subject D, trial 3
A
B
C
angle (in degrees)
angle difference (in degrees)
trend difference (in degrees)
frame number

Subject D, trial 4

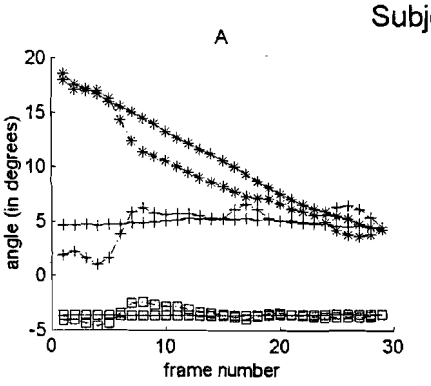

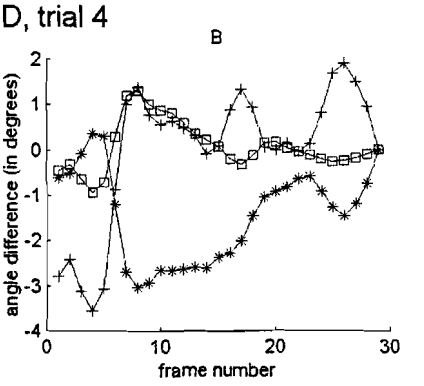

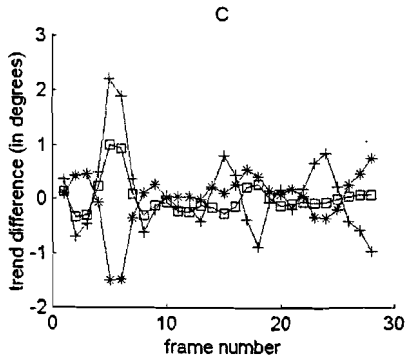

Subject E, trial 2

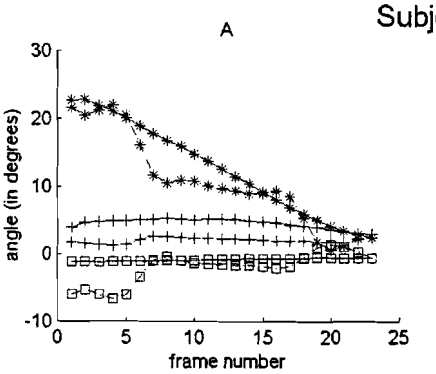

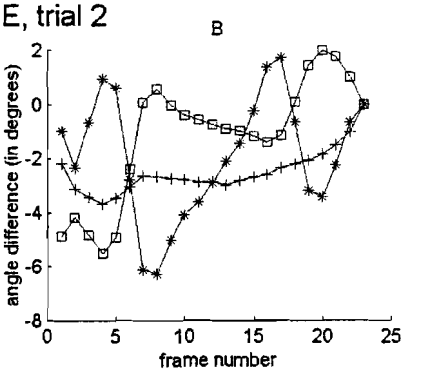

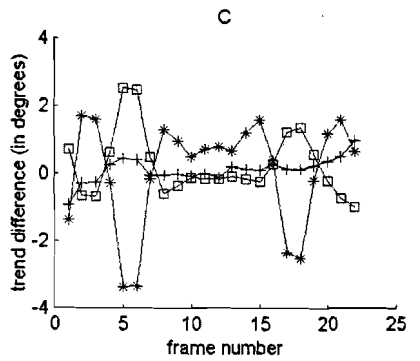

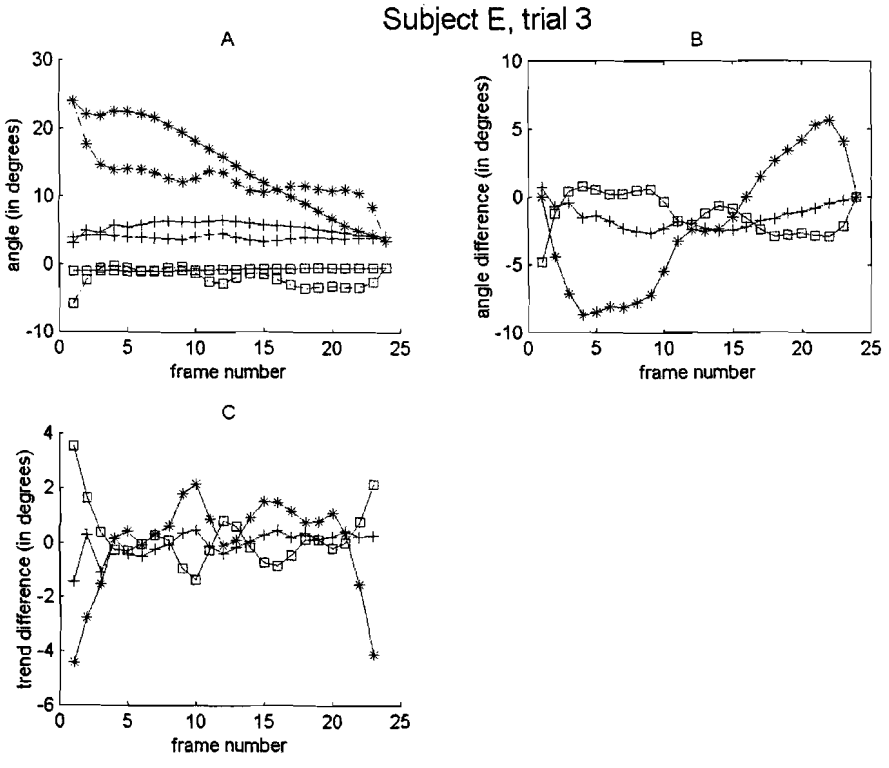
Subject E, trial 3
A
B
C
angle (in degrees)
angle difference (in degrees)
trend difference (in degrees)
frame number
Subject E, trial 5
A
B
C
angle (in degrees)
angle difference (in degrees)
trend difference (in degrees)
frame number

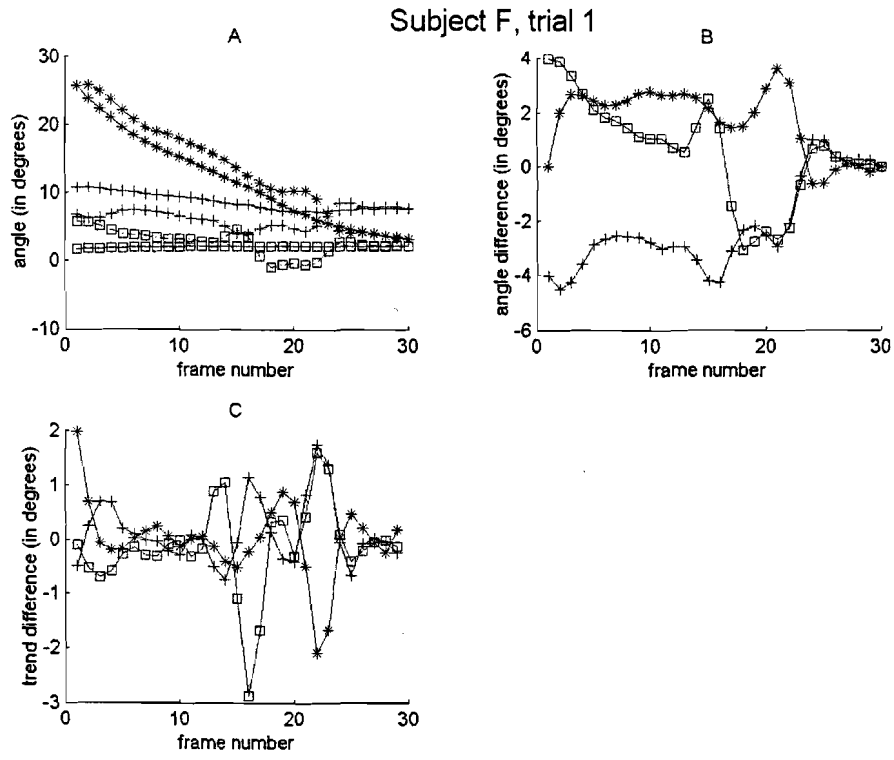
Subject F, trial 1
A
B
C
angle (in degrees)
angle difference (in degrees)
trend difference (in degrees)
frame number

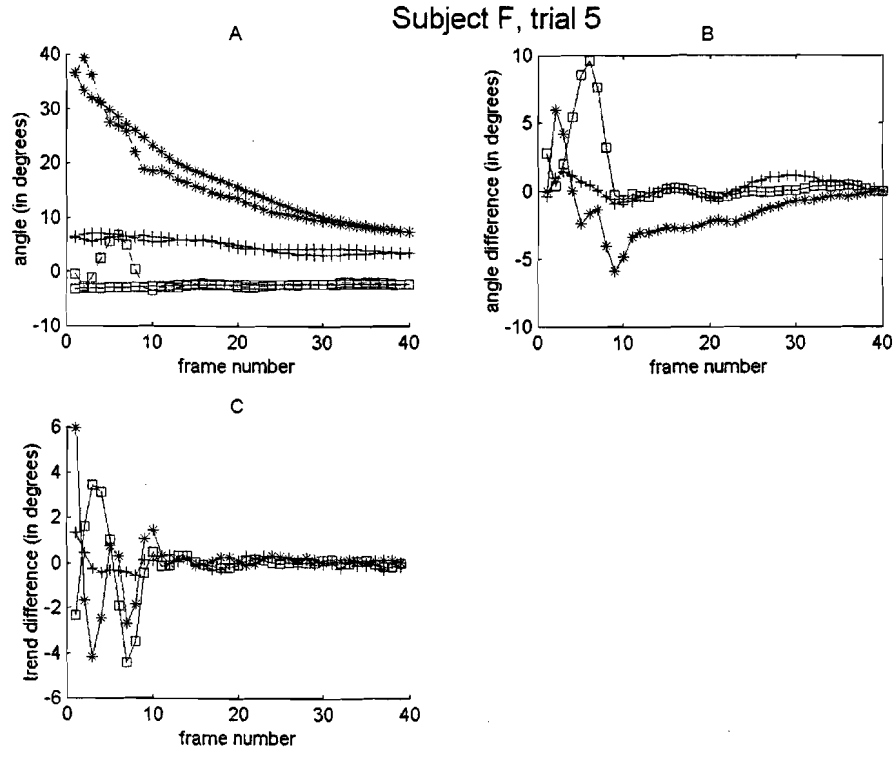
Subject F, trial 5
A
B
C
angle (in degrees)
angle difference (in degrees)
trend difference (in degrees)
frame number